

Taiwan river muds from source to sink: Provenance control, inherited weathering, and offshore dispersal pathways

Kalyani Nayak ^{a,*}, Eduardo Garzanti ^{a,*}, Andrew Tien-Shun Lin ^b, Sebastien Castelltort ^c

^a Laboratory for Provenance studies, Department of Earth and Environmental Sciences, University of Milano-Bicocca, Milano, Italy

^b Department of Earth Sciences, National Central University, Taiwan

^c Department of Earth Sciences, University of Geneva, Geneva, Switzerland

ARTICLE INFO

Article history:

Received 4 April 2022

Received in revised form 16 June 2022

Accepted 25 June 2022

Available online 05 July 2022

Editor: Dr. Catherine Chagué

Keywords:

Provenance analysis
Clay minerals
Mud geochemistry
Physical erosion
Chemical weathering
Taiwan Island

ABSTRACT

Clay mineralogy and geochemistry of river muds around Taiwan Island reveal dominant provenance control. Abundant illite with subordinate chlorite in the western, northern, and southern parts of the island are derived from Cenozoic mudrocks of the axial Slate Belt and Western Foothills. In eastern Taiwan, chlorite is most common in muds generated from the Tananao Complex, whereas smectite is produced by erosion of arc andesites of the Coastal Range. Kaolinite occurs in minor amounts in western Taiwan, where it is mostly recycled from mudrocks originally generated in mainland China and accumulated along the Chinese passive margin before being tectonically accreted in the Western Foothills of the Taiwan thrust belt. Only locally in more humid regions of northern Taiwan may moderate kaolinite content associated with relatively high illite chemistry index hint at present kaolinite formation. Mineralogical and geochemical indications of weathering are thus considered to be mostly inherited rather than indicative of present climatic and geomorphological conditions.

A comparison of clay-mineral assemblages in Taiwan river muds and offshore deep-sea clays allows us to trace sediment transport from the land to the deep-sea. Mostly illite is supplied to the Taiwan Strait and the South China Sea, whereas subequal amounts of illite and chlorite are delivered to the Ryukyu forearc basin from eastern Taiwan rivers draining the Tananao Complex. Smectite from Coastal Range andesites is transferred via the Xiuguluan River and Chimei Canyon directly to the Ryukyu trench. Additional amounts of smectite produced in the Ryukyu and Luzon arcs are transported southward to the Ryukyu forearc basin and northward by the Kuroshio Current, northwestward to the northern South China Sea and northeastward to the Huatung Basin and Okinawa Trough.

© 2022 Elsevier B.V. All rights reserved.

1. Introduction

Assessing the variables that control continental erosion is essential for a better understanding of the complex geological and geomorphological processes that lead to silicate, carbonate, and sulfide weathering, thus impacting on the carbon cycle and in turn on global climate (Raymo et al., 1988; Gaillardet et al., 1999; Clift et al., 2006a; Liu et al., 2007b). Both endogenous and exogenous processes are particularly intense in southeastern Asia (Clark et al., 2004; Liu et al., 2005), and especially in Taiwan, where tectonic and climatic hazards are extreme and erosion rates are among the highest on Earth (Schoenbohm et al., 2004; Clift et al., 2006b). River systems in the region have consequently a very high sediment load, accounting for

two-thirds of total suspended sediments supplied to the world's oceans (Milliman and Syvitski, 1992; Summerfield and Hulton, 1994).

Taiwan Island is located at the tectonic boundary between the colliding Eurasian and Philippine Sea plates, leading to rapid rock-uplift rates up to 5–7 mm/year and more (Dadson et al., 2003; Fuller et al., 2006; Simoes et al., 2012; Resentini et al., 2017). The Taiwan orogen connects two subduction systems: the Ryukyu subduction zone in the northeast, where the Philippine Sea Plate is subducting beneath the Eurasian Plate, and the Manila subduction zone in the south, where the South China Sea is dragged beneath the Philippine Sea Plate (Fig. 1). Tectonic deformation and seismicity are consequently intense both inland and offshore Taiwan.

Besides tectonic activity, high rates of sediment production and transport inland and offshore are fostered by frequent typhoons, heavy rainfall, and intense oceanic circulation, which make the region an unexcelled location for studying the impact of these processes on sediment generation and dispersal to the deep-sea. Only a few mineralogical and geochemical studies have been carried out so far to trace

* Corresponding authors.

E-mail addresses: kalyani.nayak@unimib.it (K. Nayak), eduardo.garzanti@unimib.it (E. Garzanti).

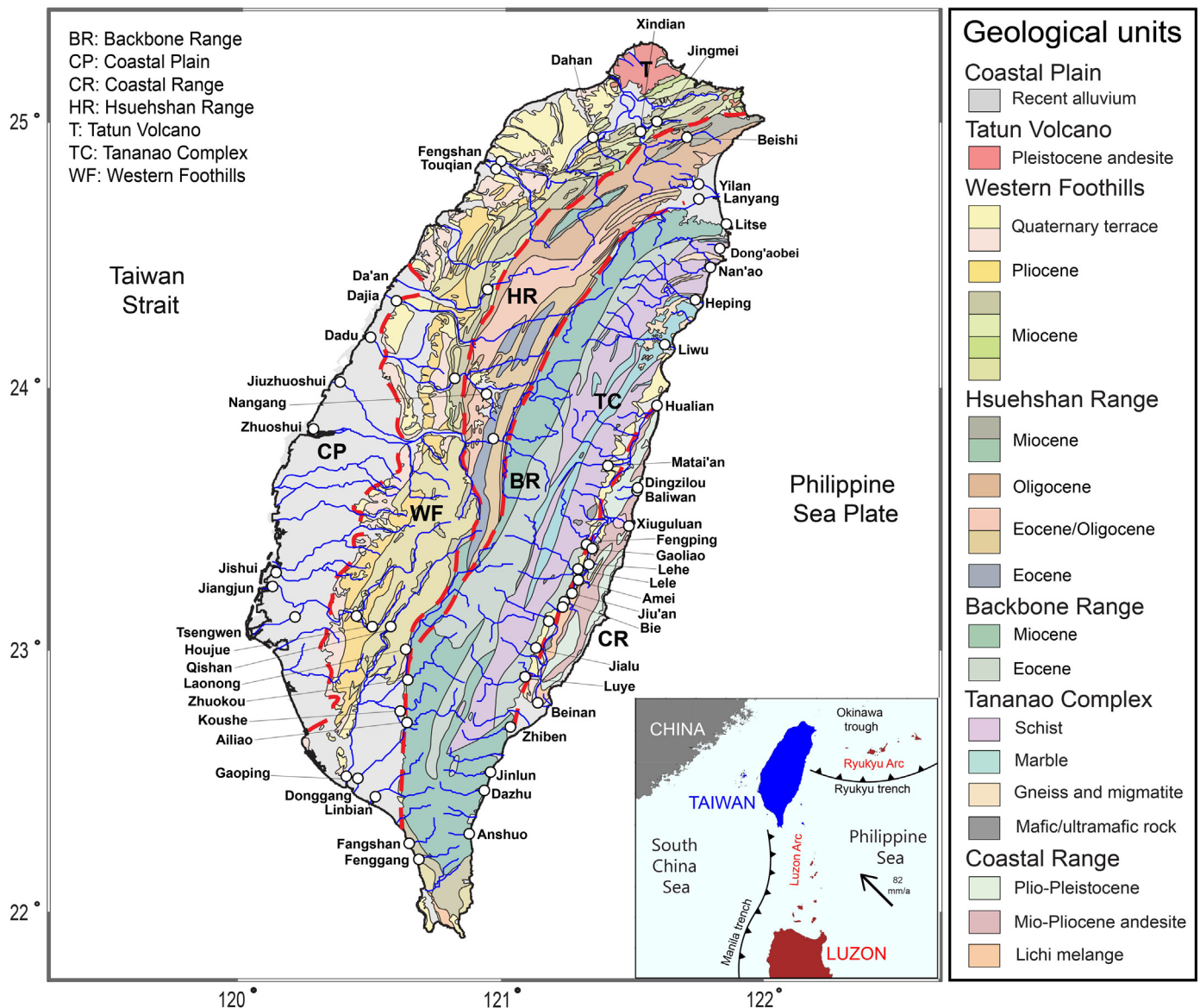


Fig. 1. Geological map of Taiwan (after Chen, 2000) showing the sites of mud samples analyzed in this study.

patterns and pathways of sediment transfer within and offshore Taiwan (e.g., Selvaraj and Chen, 2006; Z. Liu et al., 2008b; Li et al., 2012). The present article illustrates the distribution of clay minerals in river muds all around Taiwan Island and combines illite chemistry index and illite crystallinity data with elemental geochemistry to evaluate the relative importance of physical versus chemical erosion, thus shedding light on regimes of weathering and sediment generation in the Taiwan orogen. Sediment transfer from Taiwan to the Philippine and northern South China seas is traced based on clay-mineral data from Nayak et al. (2021).

2. Geological and geomorphological framework

2.1. Geology of Taiwan

The Taiwan doubly-vergent orogenic wedge was generated during subduction of the Chinese continental margin beneath the Luzon volcanic arc since the late Miocene (Suppe, 1981; Byrne et al., 2011). The frontal part of the fold-thrust belt is represented by the Western Foothills, where Oligocene-Miocene sediments deposited originally along the passive margin of the Chinese mainland are overlain by 4 km-

thick Pliocene-Quaternary foreland-basin deposits shed from erosion of the uplifting Taiwan orogen (Nagel et al., 2014, 2018; Lin et al., 2021). The most recent part of the foreland basin is the Coastal Plain, where alluvial and terrace deposits are underlain by Pliocene-Pleistocene marine sediments (Fig. 1) (Lin and Watts, 2002).

The central part of the Taiwan orogen includes polymetamorphic basement rocks of the Tananao Complex and very low-grade mudrocks of the Slate Belt exposed in the Hsuehshan and Backbone ranges. These mudrocks represent the distal part of the thick succession deposited along the Chinese continental margin during Paleogene extension associated with the roll-back of the westward-subducting Paleopacific plate (Ernst and Jahn, 1987; Lin et al., 2003). Mudrocks and intercalated sandstones exposed in the Hsuehshan Range document sedimentation through the Eocene-Oligocene (Teng and Lin, 2004), whereas post-rift Miocene sediments underlain by Eocene slates and metasandstones non-conformably overlying Tananao basement rocks are exposed in the Backbone Range (Yu et al., 2013). The Tananao Complex includes the inboard Tailuko Belt, where marbles, metabasites, metacherts, and schists are intruded by Upper Cretaceous (85–90 Ma) granites in the north (Yui et al., 2012), and the outboard Yuli Belt, consisting of black schists with blocks of serpentinite and metabasite that underwent

subduction-related high-pressure metamorphism (Keyser et al., 2016; Huang et al., 2021).

The Longitudinal Valley marks the plate boundary (Fig. 1) (Chang et al., 2000). Farther to the east, the Coastal Range represents the northern extension of the Luzon arc, where basaltic andesite to dacite lava flows and ignimbrites were generated during eastward subduction of the Eurasian Plate beneath the Philippine Sea Plate in the Miocene (Defant et al., 1990; Lai et al., 2017). These volcanic rocks are covered by a 6-km-thick post-collisional Pliocene-Pleistocene siliciclastic succession (Dorsey, 1988).

Shortening is no longer active in northern Taiwan, where the orogen is disrupted by normal faults associated with southwestward

propagation and roll-back of the Ryukyu subduction zone and consequent intra-arc rifting and back-arc spreading in the Okinawa Trough (Teng, 1996). As part of the northern Taiwan volcanic zone, the Pleistocene Tatun volcano mostly erupted basaltic-andesite and andesite lavas with subordinate pyroclastic deposits (Wang et al., 2004; Shellnutt et al., 2014).

2.2. Geomorphology and climate

The island of Taiwan lies at tropical latitudes between 21°54'N and 25°18'N and has a mild climate throughout the year with average annual temperatures ranging from 22 °C in the north to 24 °C in the

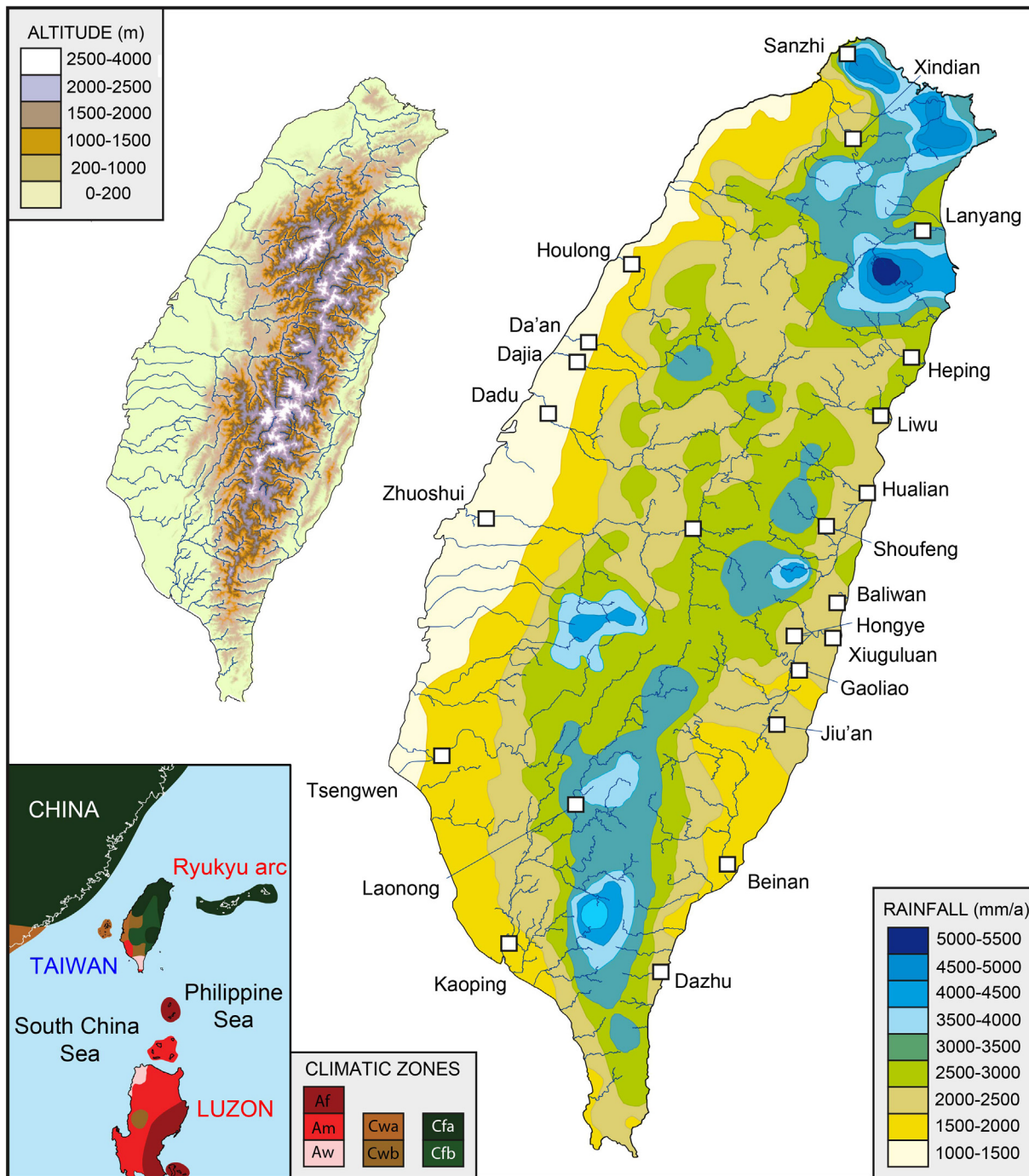


Fig. 2. Topographic and rainfall maps of Taiwan. Samples of river sands studied by Garzanti and Resentini (2016) are indicated. Digital elevation map after ASTER GDEM (<http://gdem.ersdac.jspacesystems.or.jp>). Climatic zones (Kottek et al., 2006): A = equatorial; C = warm temperate. Precipitation: f = fully humid; m = monsoonal; w = winter dry. Temperature: a = hot summer; b = warm summer.

south. In winter, frost or snow may occur on the high mountains, whereas temperatures may reach 38 °C in summer. Numerous mountain peaks on the island reach above 3000 m a.s.l. and up to 3952 m a.s.l. on the summit of Jade Mountain. Annual rainfall, 65 % and 90 % of which concentrated between May and October, is on average 2.0–2.5 m along the eastern coast, reaches 3 m in the central range and in the north, and decreases to 1.5 m or less along the western coast. The northern foothills and mountain areas may receive up to 5 m or even 6 m of rain annually (Fig. 2). Typhoons from the Pacific Ocean hit the island four to five times per year on average, mostly between July and September, bringing >2 m of torrential rain and triggering multiple

massive mudslides and rockslides (e.g., Dadson et al., 2005; Hovius et al., 2011; Montgomery et al., 2014). Because of such climatic conditions coupled with rapid tectonic deformation, extreme relief, and frequency of high-magnitude earthquakes, erosion rates are among the highest on Earth, reaching up to a few cm/year locally (e.g., Fuller et al., 2006; Resentini et al., 2017; Deng et al., 2020, 2021).

2.3. Clays on land and offshore

Processes of physical erosion in a weathering-limited regime are dominant in Taiwan, as indicated by geochemical and mineralogical

Table 1

Clay mineralogy of Taiwan river muds. Provenance groups (Prov.) based on sampling criteria are corroborated by petrographic data (Resentini et al., 2017): CR = Coastal Range; S = Slate belt (NE, northeast; S, south; W, west); TC = Tananao Complex. Major rivers with mixed sediment composition: E = eastern rivers, N = northern rivers; W = western rivers.

River	Site	Prov.	Smectite	Illite	Chlorite	Kaolinite	Illite crystallinity	Illite chemistry index
			%	%	%	%	$^{\circ}\Delta 2\theta$	
Dahan	Sanying	N	50	33	12	5	0.30	0.25
Xindian	Xindian	N	2	72	24	2	0.35	0.32
Jingmei	Xiangtoupou	N	35	34	16	16	0.41	0.42
Beishi	Pinglin	N	4	78	16	2	0.44	0.32
Yilan	Yilan	S (NE)	1	76	23	0	0.36	0.31
Lanyang	Erjie	S (NE)	1	75	24	0	0.34	0.30
	Litse	TC	0	65	35	0	0.28	0.21
Dong'aobei	Dong'ao	TC	7	35	58	0	0.18	0.23
Nan'ao	Nan'ao	TC	0	56	44	0	0.20	0.31
Heping	Heping	TC	3	69	26	2	0.24	0.20
Liwu	Tailuko	TC	4	48	48	0	0.26	0.19
Hualian	Renhe	E	8	45	47	0	0.20	0.19
Matai'an	Matai'an	TC	0	26	74	0	0.27	0.15
Dingzilou	Fengbin	CR	53	32	13	2	0.26	0.27
Baliwan	Fengbin	CR	31	44	25	0	0.31	0.35
Xiuguluan	Dagangkou	E	40	32	25	3	0.19	0.28
Fengping	Taiping	TC	0	39	61	0	0.24	0.22
Gaoliao	Gaoliao	CR	85	10	5	0	0.38	0.25
Lehe	Lehe	CR	54	29	14	3	0.34	0.27
Lele	Kecheng	TC	3	57	37	3	0.17	0.25
Amei	Wanning	CR	79	13	8	0	0.37	0.27
Jiu'an	Futian	CR	97	2	1	0	0.28	0.29
Bie	Fuli	CR	46	32	18	4	0.45	0.45
Xiuguluan	Funan	E	23	48	29	0	0.29	0.25
Beinan	Chishang	TC	0	55	45	0	0.25	0.30
Jialu	Jiana	TC	0	71	29	0	0.19	0.20
Luye	Luye	TC	0	64	36	0	0.27	0.28
Beinan	Taidong	E	5	58	35	2	0.18	0.28
Zhiben	Zhiben	S (S)	0	73	27	0	0.26	0.20
Jinlun	Jinlun	S (S)	0	72	28	0	0.21	0.18
Dazhu	Daxi	S (S)	0	69	31	0	0.23	0.28
Anshuo	Daren	S (S)	0	76	24	0	0.35	0.24
Fenggang	Fenggang	S (S)	0	72	28	0	0.41	0.25
Fangshan	Fangshan	S (S)	0	68	32	0	0.40	0.25
Linbian	Linbian	S (S)	0	73	27	0	0.31	0.32
Donggang	Xinyuan	S (S)	0	72	28	0	0.26	0.18
Kaoping	Daliao	S (S)	0	65	28	7	0.32	0.29
Ailiao	Sandimen	S (S)	0	65	35	0	0.23	0.28
Koushe	Guangxing	S (S)	0	71	29	0	0.22	0.27
Zhuokou	Dajin	S (S)	0	66	34	0	0.17	0.32
Laonong	Liugui	S (S)	0	70	26	4	0.28	0.29
Qishan	Jiaxian	S (S)	0	67	28	6	0.50	0.29
Houjue	Toufen	W	3	61	28	8	0.37	0.29
Tsengwen	Yujing	W	43	39	14	4	0.44	0.25
Tsengwen	Xigang	W	17	57	19	7	0.36	0.31
Jiangjun	Jiangjun	W	10	60	21	9	0.38	0.34
Jishui	Beimen	W	19	54	20	7	0.36	0.32
Zhuoshui	Dacheng	S (W)	1	66	30	3	0.29	0.24
Jiuzhuoshui	Maiyucuo	S (W)	0	65	35	0	0.27	0.33
Dadu	Longjing	W	33	46	13	8	0.28	0.34
Zhuoshui	Shuanglong	S (W)	1	72	27	0	0.15	0.13
Nangang	Puli	S (W)	0	69	25	6	0.30	0.36
Dadu	Guigou	S (W)	4	61	32	3	0.30	0.29
Da'an	Xiangbi	S (W)	0	83	17	0	0.34	0.23
Dajia	Qingshui	W	33	48	14	6	0.43	0.28
Touqian	Xizhou	W	28	43	21	8	0.33	0.32
Fengshan	Zhubei	W	49	30	15	7	0.33	0.38

features including fresh detrital feldspars and clay-mineral assemblages dominated by illite and chlorite with minor smectite and rare kaolinite (Dorsey et al., 1988; Chamley et al., 1993; Li et al., 2012; Nagel et al., 2014). Clay mineral studies documented how Taiwan offshore areas receive sediment from various sources, including rivers in southeast China and the Luzon arc system. Sediment production in Taiwan and transport offshore is fostered by extreme processes such as earthquakes, typhoons and rainstorms, coupled with intense oceanic circulation (Liu et al., 2010; Das et al., 2021; Nayak et al., 2021).

Clays generated on Taiwan Island are mainly illite and chlorite, minerals that largely result from the disintegration of phyllosilicates during physical erosion of source rocks (Biscaye, 1965; Boulay et al., 2003). Illite is mostly derived from slates of the Backbone and Hsuehshan ranges and from mudrocks of the Western Foothills, whereas chlorite is largely produced from erosion of Tananao Complex metamorphic rocks (Li et al., 2012).

As a weathering product of volcanic rocks including glass and ferromagnesian silicates, smectite is dominant in rivers draining arc andesites exposed in the Coastal Range (Chamley et al., 1993). Smectite is also common offshore eastern and southern Taiwan, where it is supplied from volcanic rocks of the Ryukyu and Luzon arcs (Liu et al., 2003; Z. Liu et al., 2008b; Nayak et al., 2021).

Kaolinite, which is characteristic of lateritic soils formed at hot-wet subequatorial latitudes (Chamley, 1989), is minor in Taiwan river muds. Kaolinite does occur in well-drained perhumid forest soils of

Taiwan highlands (Pai et al., 2007), where it is largely trapped in mountain lakes (Li et al., 2012). Kaolinite is found in the northern South China Sea, where it is held to be mainly derived from kaolinite-rich Pearl River sediments (Liu et al., 2007a, 2007b; He et al., 2020).

3. Methods

During our field campaign in October 2012, we collected 106 modern sands and 57 freshly deposited muds from riverbanks, river bars, and beaches all around the island of Taiwan. All sand samples have been studied for their mineralogy and a selected set for their geochemistry as well (Garzanti and Resentini, 2016; Resentini et al., 2017), whereas the mineralogical and geochemical study of the 57 mud samples represents the core of the present study. This sample set is notably wider than considered in most previous studies focusing on either clay mineralogy (e.g., Li et al., 2012) or mud geochemistry (e.g., Selvaraj and Chen, 2006) and covers the whole of Taiwan, being representative of suspended load not only in all major rivers but also in several minor rivers draining specific geological units exclusively, chosen to characterize at best the end-member signatures of detritus produced from all different tectonic domains and source-rock lithologies. Full information on sampling sites is provided in Appendix Table A1. Grain size of 26 mud samples was determined, after removing organic matter and carbonates, with a Beckman Coulter LS13 320 laser diffraction particle-size analyzer at the Department of Earth Sciences of the National Central

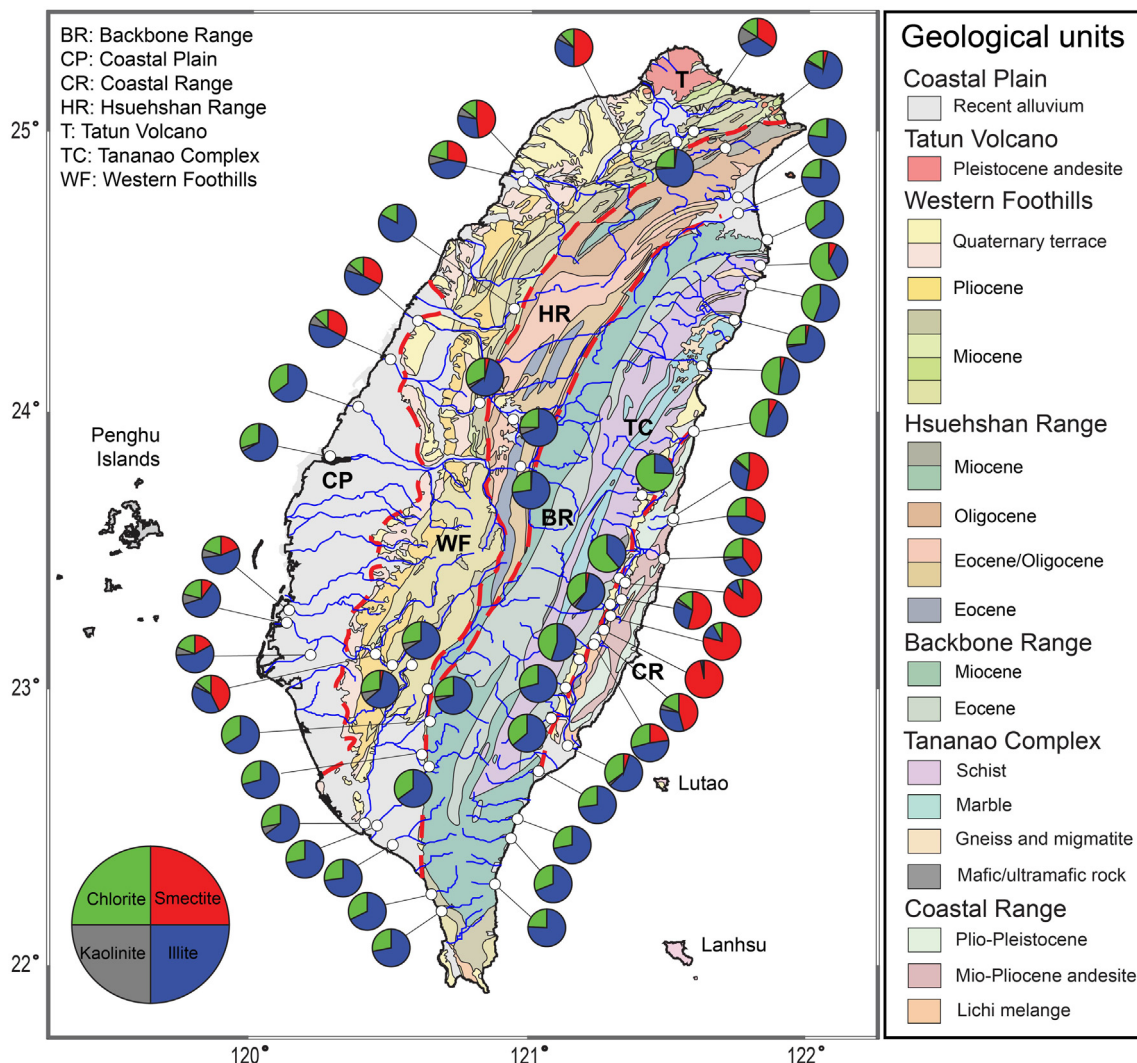


Fig. 3. Clay-mineral distribution in the studied Taiwan river muds.

Table 2
Geochemistry of Taiwan river muds and main chemical indices.

River	SiO ₂ wt%	Al ₂ O ₃ wt%	Fe ₂ O ₃ wt%	MgO wt%	CaO wt%	Na ₂ O wt%	K ₂ O wt%	Rb ppm	Sr ppm	Ba ppm	Sc ppm	La ppm	Nd ppm	Th ppm	Zr ppm	V ppm	Cr ppm	Ni ppm	CIA	WIP	α ^{Al} Mg	α ^{Al} Ca	α ^{Al} Na	α ^{Al} K	α ^{Al} Sr
Dahan	59.8	18.7	7.3	3.1	5.0	1.1	3.4	151	156	565	13.5	58	27	9.5	428	101	60	50	57	59	0.9	0.9	4.1	1.1	2.6
Xindian	64.4	20.2	6.8	2.3	0.2	1.3	3.3	149	94	570	11.7	45	28	9.9	301	99	63	52	78	47	1.3	21.1	3.6	1.2	4.7
Jingmei	61.6	19.9	9.0	2.1	0.8	1.2	3.3	151	159	738	13.2	47	36	11.4	553	111	73	61	76	45	1.4	6.3	4.0	1.2	2.7
Beishi	65.6	19.8	6.1	1.9	0.4	1.1	3.4	147	117	624	12.4	44	28	10.3	560	100	63	51	77	45	1.6	12.2	4.3	1.2	3.7
Yilan	62.5	20.6	7.8	2.5	0.4	1.3	3.4	156	92	565	12.7	61	29	9.6	221	102	60	52	78	48	1.3	14.9	3.8	1.2	4.9
Lanyang	59.3	22.2	8.3	2.2	0.9	1.4	3.8	177	129	573	13.1	49	29	9.4	265	103	61	53	74	53	1.5	6.1	3.7	1.2	3.8
Litse beach	58.1	19.4	6.8	2.4	0.7	4.2	3.4	150	129	488	13.3	57	27	9.2	191	100	61	48	63	76	1.2	7.0	1.1	1.2	3.3
Dong'aobei	52.9	18.7	11.4	8.6	2.3	1.3	2.6	87	86	528	17.1	62	28	8.3	209	134	115	77	70	62	0.3	2.0	3.5	1.4	4.8
Nan'ao	58.4	21.0	7.3	3.0	2.6	1.9	4.3	175	179	589	13.2	33	27	9.4	262	100	61	49	64	68	1.1	2.1	2.6	1.0	2.6
Heping	60.9	19.0	7.0	2.7	3.4	1.9	3.3	140	184	542	12.3	37	27	9.3	271	97	57	51	61	61	1.1	1.4	2.3	1.2	2.3
Liwu	60.7	13.5	6.0	3.7	10.3	1.9	2.3	86	252	533	14.3	29	24	9.0	157	98	59	52	36	73	0.6	0.3	1.7	1.2	1.2
Hualian	56.0	12.6	6.5	4.1	15.3	1.7	2.2	85	210	545	15.1	60	23	8.9	200	99	63	53	28	84	0.5	0.2	1.7	1.2	1.3
Matai'an	40.2	16.9	7.9	8.5	20.3	1.9	2.5	92	208	632	17.1	51	23	8.5	219	106	68	52	29	113	0.3	0.2	2.1	1.3	1.8
Dingzilou	61.9	18.4	7.2	3.9	2.7	1.5	3.0	130	139	563	13.0	49	28	9.6	316	106	78	67	65	56	0.7	1.8	2.9	1.2	2.9
Baliwan	65.7	16.9	6.5	3.3	1.8	1.8	2.7	114	120	574	12.5	50	28	9.7	199	99	68	62	66	53	0.8	2.4	2.2	1.2	3.1
Xiuguluan	58.4	17.5	6.5	3.7	7.8	1.8	2.9	127	197	560	13.9	71	25	9.5	242	98	68	58	47	71	0.7	0.6	2.2	1.2	1.9
Fengping	53.8	20.0	8.4	5.2	5.4	2.1	3.1	123	172	508	16.0	64	27	9.2	291	114	82	54	55	73	0.6	0.9	2.2	1.3	2.5
Gaoliao	60.8	18.7	7.6	4.3	3.1	1.6	2.5	107	139	519	13.9	31	27	9.5	303	109	77	58	64	54	0.7	1.5	2.8	1.5	2.9
Lehe	63.2	18.2	7.1	3.5	2.1	1.6	3.0	123	116	566	13.0	51	28	9.7	239	103	66	58	67	54	0.8	2.2	2.7	1.2	3.4
Lele	58.0	16.2	5.8	2.8	11.3	1.7	3.0	127	246	528	13.2	28	24	9.2	214	89	56	49	38	77	0.9	0.4	2.3	1.1	1.4
Amei	61.8	18.8	7.1	3.8	2.6	1.6	2.8	113	138	531	12.9	43	27	9.5	312	104	72	56	66	54	0.8	1.8	2.8	1.4	3.0
Jiu'an	59.3	16.8	6.7	6.3	6.2	2.5	1.3	40	210	517	14.5	25	25	9.3	118	105	81	61	51	66	0.4	0.7	1.6	2.6	1.8
Bie	61.2	18.6	7.2	3.4	3.6	1.4	3.0	129	152	560	13.5	46	27	9.5	254	106	67	55	62	56	0.8	1.3	3.2	1.3	2.7
up. Xiuguluan	62.2	18.6	6.6	2.5	3.2	2.0	3.2	129	179	527	13.2	93	28	9.9	434	99	65	51	61	60	1.1	1.5	2.2	1.2	2.3
upper Beinan	58.8	19.9	6.8	3.3	4.5	1.7	3.7	159	182	571	13.1	17	26	9.4	154	95	55	44	58	67	0.9	1.1	2.8	1.1	2.4
Jialu	61.8	19.9	7.5	2.3	1.1	1.8	4.1	165	151	462	13.2	68	28	9.8	285	104	79	52	69	60	1.3	4.8	2.6	1.0	2.9

Luye	59.9	21.3	6.7	2.6	2.3	1.9	4.0	178	172	598	12.8	33	27	9.5	161	96	58	48	65	64	1.2	2.3	2.7	1.1	2.7
Beinan	63.7	17.8	6.0	2.5	3.9	1.7	3.1	133	177	574	12.5	48	26	9.8	187	93	58	47	58	58	1.1	1.2	2.4	1.2	2.2
Zhiben	69.7	13.9	4.5	1.6	3.9	2.4	2.8	93	185	582	11.4	41	26	9.9	290	85	52	47	51	60	1.3	0.9	1.3	1.0	1.6
Jinlun	63.9	18.3	6.2	2.2	1.8	1.8	4.4	189	109	430	13.0	77	26	10.2	259	96	58	47	63	64	1.2	2.6	2.4	0.8	3.7
Dazhu	64.1	18.8	6.5	2.1	1.7	1.8	3.7	152	141	606	11.9	58	27	9.7	191	96	58	51	66	57	1.4	2.9	2.4	1.0	2.9
Anshuo	63.6	20.3	7.4	2.0	0.5	1.1	3.5	168	107	539	14.7	67	29	10.8	501	113	70	54	77	46	1.6	10.6	4.4	1.2	4.1
Fenggang	63.2	20.0	7.7	2.3	0.9	1.2	3.2	145	100	568	12.9	34	28	9.6	281	106	64	52	76	46	1.4	5.8	3.9	1.3	4.4
Fangshan	66.1	18.2	6.4	2.2	1.5	1.4	2.8	124	98	564	12.0	35	28	9.7	264	98	60	51	71	46	1.3	3.1	3.0	1.3	4.1
Linbian	59.4	22.1	8.1	2.3	1.2	1.5	3.7	178	128	576	13.1	49	29	9.3	228	104	63	52	73	54	1.5	4.6	3.6	1.2	3.8
Donggang	62.9	20.3	7.6	1.9	0.5	1.3	3.6	162	105	388	14.0	51	27	10.0	197	105	75	52	77	48	1.6	10.2	3.7	1.1	4.2
Kaoping	61.2	20.0	7.3	2.6	2.4	1.3	3.6	163	141	568	13.0	35	28	9.5	228	99	59	51	67	55	1.2	2.2	3.7	1.1	3.1
Ailiao	62.0	19.6	6.8	2.2	2.5	1.8	3.8	167	149	587	12.2	39	27	9.5	157	94	54	48	63	61	1.4	2.0	2.5	1.0	2.9
Koushe	60.5	21.2	7.9	2.2	1.5	1.6	3.5	167	145	565	12.9	50	29	9.4	219	100	60	53	71	53	1.5	3.7	3.1	1.2	3.2
Laonong	64.0	18.1	6.6	2.3	2.7	1.4	3.3	126	130	492	12.2	48	26	9.5	264	95	59	48	63	54	1.2	1.7	3.0	1.1	3.0
Qishan	58.9	21.8	8.2	3.0	1.5	0.8	4.2	194	119	568	13.8	65	29	9.2	167	107	67	53	73	54	1.1	3.7	6.5	1.0	4.0
Houjue	60.8	20.1	7.8	2.8	2.2	1.1	3.5	160	139	560	13.1	60	28	9.5	237	107	63	51	69	52	1.1	2.3	4.4	1.2	3.2
up.Tsengwen	64.1	18.1	7.1	2.6	2.2	1.2	3.1	142	129	573	13.1	68	28	9.8	240	103	60	50	67	50	1.1	2.1	3.4	1.2	3.1
Tsengwen	59.3	21.4	8.3	2.8	1.6	1.1	3.9	179	122	559	13.1	63	28	9.4	183	104	63	51	72	54	1.2	3.4	4.7	1.1	3.8
Jiangjun	60.1	19.6	8.1	2.9	1.2	1.6	3.5	158	151	562	13.5	62	29	9.7	283	108	79	53	74	53	1.1	4.0	2.9	1.1	2.8
Jishui	63.7	19.3	6.9	2.7	0.9	1.4	3.3	147	111	567	12.8	44	28	9.6	308	102	67	51	74	49	1.1	5.7	3.3	1.2	3.8
Zhuoshui	62.7	19.2	7.1	2.2	2.2	1.6	3.4	156	152	571	12.4	50	28	9.5	275	96	57	50	66	54	1.3	2.2	2.8	1.1	2.8
Jiuzhuoshui	58.5	22.3	8.2	2.4	1.1	1.4	4.1	203	143	576	13.5	42	28	9.5	195	105	76	59	75	55	1.4	5.3	3.8	1.1	3.4
Dadu	62.3	19.9	8.1	2.3	0.9	1.2	3.4	163	115	564	13.1	51	29	9.5	271	104	61	52	74	48	1.4	5.6	3.8	1.2	3.8
up. Zhuoshui	61.4	21.0	7.0	2.3	1.6	1.6	3.7	168	160	583	12.7	33	27	9.5	191	98	59	50	69	56	1.4	3.3	3.0	1.2	2.9
Nangang	63.2	21.9	6.6	1.9	0.2	0.7	4.0	217	87	594	12.3	32	27	10.2	280	99	59	51	81	45	1.8	26.5	7.4	1.1	5.5
Dadu	62.4	17.6	7.3	2.0	4.5	1.1	3.3	164	166	521	13.2	50	27	9.6	622	99	65	50	58	55	1.3	1.0	3.6	1.1	2.3
Da'an	65.4	19.5	5.8	1.6	1.3	0.9	3.8	185	126	592	11.5	33	28	10.1	367	90	53	49	72	48	1.9	3.9	5.1	1.0	3.4
Dajia	65.1	19.4	6.5	1.9	1.4	0.9	3.4	162	111	589	11.9	39	28	10.1	293	94	59	55	73	45	1.6	3.6	5.1	1.2	3.8
Touqian	66.7	17.0	6.5	2.2	1.5	1.6	2.8	117	139	582	12.8	57	28	10.0	557	102	61	50	69	47	1.2	3.0	2.5	1.2	2.7
Fengshan	65.0	18.1	7.6	2.0	1.0	1.3	2.9	124	144	566	12.8	66	29	9.5	399	103	64	53	74	44	1.4	4.4	3.2	1.3	2.8

University of Taiwan (data and full description of analytical methods are provided in Appendix Table A2).

3.1. Clay mineralogy

The clay mineralogy of 57 mud samples was determined on $<2 \mu\text{m}$ fractions by X-ray powder diffraction (XRD) at the Department of Earth Sciences of the National Central University of Taiwan. We used a Bruker D2 Phaser X-ray diffractometer operated with an X-ray of $\text{CuK}\alpha$ at the voltage of 30 kV and 10 mA current. The clay fraction ($<2 \mu\text{m}$) was separated by centrifuging according to Stokes' law after removing carbonates and organic matter by H_2O_2 15 % and HCl 10 %. Following air-drying and ethylene-glycol solvation, clay minerals were analyzed on oriented aggregates in the range of $3\text{--}30^\circ$ (2θ), with a step size of 0.02° . XRD runs were performed two times and several samples were heated at 490°C for 2 h to validate the presence of kaolinite. Clay minerals were identified based primarily on the position of the (001) series of basal reflections. Semi-quantitative analysis of basal reflection peak areas for kaolinite + chlorite (7 Å), illite (10 Å), and smectite (15–17 Å, including mixed-layers of smectite-illite at 15–16 Å) was carried out on glycolate specimens using PeakFit software after background subtraction. Kaolinite and chlorite were discriminated according to the relative proportions given by a ratio of the 3.57 Å and 3.54 Å peak areas. The relative abundances of clay minerals are reported in percentages. Weighting factors proposed by Biscaye (1965) were not employed to obtain clay-mineral percentages (Liu et al., 2010). Illite crystallinity and Illite chemistry indices were calculated on ethylene-glycolate samples as the full width at half maximum (FWHM) of the illite 10 Å peak, and as the ratio of the 5 Å and 10 Å peak areas, respectively. Key mineralogical data are illustrated in Table 1 and Fig. 3; full information is provided in Appendix Table A3.

3.2. Mud geochemistry

The concentration of major elements and selected trace elements were determined on the $<37 \mu\text{m}$ fraction of 56 bulk-mud samples using a Bruker S8 TIGER X-ray fluorescence (XRF) spectrometer at the Department of Earth Sciences of the National Central University of Taiwan. For each sample, 9 g of sediment were mixed with 9 Mahlhilfe grinding aid tablets and ground together. Using an automated fusion

machine, 10 g of the powdered mixture were employed to make a pressed powder pellet, which was then placed in a holder and subject to examination.

Weathering intensity and other controls on geochemical composition are best detangled if each single mobile element E is considered separately, by comparing its concentration to that of non-mobile Al in our samples versus the UCC standard composition (Taylor and McLennan, 1995; Rudnick and Gao, 2003): $\alpha^{\text{AlE}} = (\text{Al}/\text{E})_{\text{sample}}/(\text{Al}/\text{E})_{\text{UCC}}$ (Garzanti et al., 2013a). Chemical indices traditionally used to estimate weathering include the CIA = $100 \cdot \text{Al}_2\text{O}_3/(\text{Al}_2\text{O}_3 + (\text{CaO} - 3.33 \cdot \text{P}_2\text{O}_5) + \text{Na}_2\text{O} + \text{K}_2\text{O})$ (Nesbitt and Young, 1982) and the WIP = $100 \cdot ((\text{CaO} - 3.33 \cdot \text{P}_2\text{O}_5)/0.7 + 2\text{Na}_2\text{O}/0.35 + 2\text{K}_2\text{O}/0.25 + \text{MgO}/0.9)$ (Parker, 1970), calculated using molecular proportions of mobile alkali and alkaline-earth metals corrected for CaO in apatite. None of these indices, however, can be confidently used as a proxy of present weathering conditions because they depend primarily on the lithology of source rocks and on other factors as well, including recycling, grain size, and hydraulic sorting (Shao et al., 2012; Garzanti et al., 2021a). The WIP, in particular, merely measures the amount of a set of mobile elements that decreases rapidly wherever quartz is added to the sediment even in the absence of weathering, making the WIP an index of quartz recycling more than an index of weathering. Because the CIA is unaffected by quartz dilution, the CIA/WIP diagram allows us to discriminate the weathering effect from the recycling effect (Garzanti et al., 2019). The full geochemical dataset is provided in Appendix Table A4.

4. Taiwan river mud

In this section, we illustrate the mineralogical and geochemical composition of Taiwan river muds. The analyzed samples are all silts containing $17 \pm 14\%$ sand and $9 \pm 5\%$ clay. Also based on petrographic and mineralogical data on modern sands (Resentini et al., 2017), we distinguish three main domains and several subdomains: 1) rivers draining principally or exclusively the Coastal Range (1a), principally or exclusively the Tananao Belt (1b), and major eastern Taiwan rivers (1c); 2) rivers draining principally or exclusively the axial Slate Belt in southern (2a), northeastern (2b), and western Taiwan (2c); and, (3) other rivers of western and northern Taiwan (Tables 1 and 2; Fig. 4).

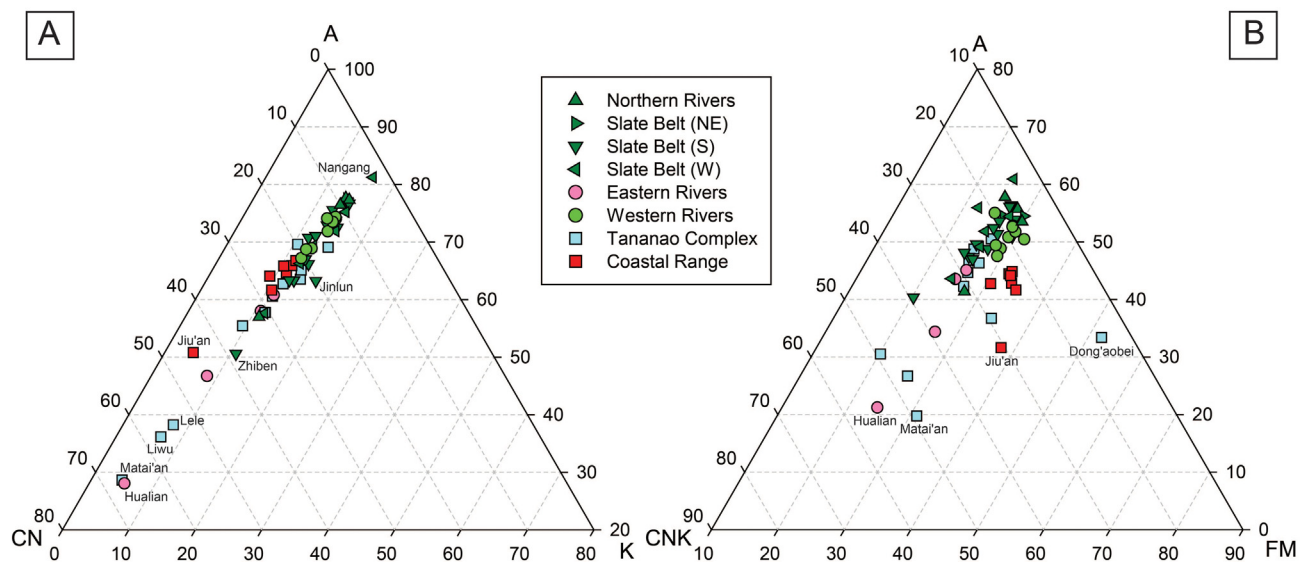


Fig. 4. Dominant provenance control on mud geochemistry (provenance groups as in Table 1). A) Data form a linear array in the ACNK diagram: muds generated from Tailuko marbles plot closer to the CN pole, muds from arc andesites plot midway, and muds rich in K_2O and especially Al from the axial Slate Belt reflect inherited weathering. B) The ACNKFM diagram better discriminates Al-rich muds derived from the Slate Belt, from muds richer in Ca, Mg, and Na derived from Tananao marbles and metabasites and from Coastal Range andesites.

4.1. Clay mineralogy

In most Taiwan river muds, including all those generated in the Slate Belt or in the Tananao belt and Western Foothills, the clay fraction ($< 2 \mu\text{m}$) consists mainly of illite (average 55 %) and chlorite (average 27 %) (Table 1; Fig. 3). Smectite is invariably dominant in muds derived from arc andesites of the Coastal Range, where it may represent up to 97 % of the clay-mineral assemblage in Jiu'an River mud, and is significant to abundant in muds of major eastern Taiwan rivers (5–8 % in Beinan and Hualian muds but 40 % in the Xiuguluan mud). Smectite, however, is locally significant also in western Taiwan rivers that do not drain volcanic rocks (e.g., 33–43 % in Dajia, Dadu, and Tsengwen muds). Chlorite is most abundant in eastern Taiwan rivers draining the Tailuko and Yuli Belts, where it may reach as high as 58 % (Dong'aobei mud), 61 % (Fengping mud), or even 74 % (Matai'an mud). Kaolinite content reaches 16 % in Jingmei River mud from northern Taiwan, is mainly 6–9 % in western Taiwan, and only ≤ 4 % in eastern Taiwan. The illite crystallinity and illite chemistry indices vary between $0.15^\circ\Delta 2\theta$ and $0.50^\circ\Delta 2\theta$, and between 0.13 and 0.45, respectively. The low illite chemistry index indicates that illite in Taiwan is mainly Fe—Mg rich.

4.2. Mud geochemistry

Geochemical trends can be clearly observed on A-CN-K (A, Al_2O_3 ; CN, $\text{CaO} + \text{Na}_2\text{O}$; K, K_2O) and A-CN-K-FM (FM, $\text{FeO} + \text{MgO}$) ternary diagrams (Nesbitt and Young, 1984, 1989). Muds carried by western, northern, and southern rivers plot closer to the Al_2O_3 apex than eastern river muds (Fig. 4), which are much richer in Mg, Ca, Na, and Sr derived from marbles and metabasites of the Tananao Complex or arc volcanic rocks of the Coastal Range (Fig. 5). CIA values uncorrected for CaO in carbonates range widely from as low as 28–38 for rivers draining Tailuko marbles (Liwu, Hualian, Matai'an, and Lele muds) to as high as 78–81 for rivers draining mudrocks of the Hsuehshan Range (Xindian, Yilan, and Nangang muds) (Table 2; Fig. 6).

5. Provenance and inherited weathering

5.1. Insights from clay mineralogy

Clay minerals are formed as a result of either physical erosion or chemical weathering, the severity of which depends on climatic conditions, water flux, biological activity, organic matter, and parent-rock mineralogy. The information provided by clay minerals, therefore, may reflect not only the climatic and geomorphological setting at the time of deposition but also refer to conditions inherited from the past via the recycling of sedimentary source rocks.

Taiwan's climate is warm and humid with dense vegetation, which fosters chemical weathering. At the same time, however, high topography and very steep slopes, strong tectonic activity, frequent landslides, and concentrated heavy rainfall induce very rapid erosion rates, leaving insufficient time for prolonged weathering (Selvaraj and Chen, 2006). As a result, physical erosion prevails in Taiwan, and clay-mineral assemblages chiefly reflect source-rock lithology, illite being derived from slates of the axial belt and shales of the Western Foothills, chlorite from schists and metabasites of the Yuli and Tailuko Belt, and smectite from Coastal Range volcanic rocks. Smectite, however, also occurs in muds carried by western Taiwan rivers that drain the Western Foothills and Coastal Plain, where volcanic rocks are lacking (Fig. 3). In soils of these relatively low-topography regions, smectite formation is favoured by poor drainage and base-rich parent material, leading to favourable chemical conditions characterized by high pH, high silica activity, and abundance of basic cations (Wilson, 1999).

The low illite crystallinity of eastern Taiwan river muds (average $0.27^\circ\Delta 2\theta$) confirms dominant physical erosion of axial belt slates, fostered by earthquakes, landslides, and extreme rainfall events (Table 1). Illite chemistry indices are somewhat higher in western Taiwan, where rivers are less steep and the climate slightly drier (Table 1). Kaolinite occurs in western Taiwan (up to 9 % of the clay-mineral assemblage), where it is inferred to be largely inherited

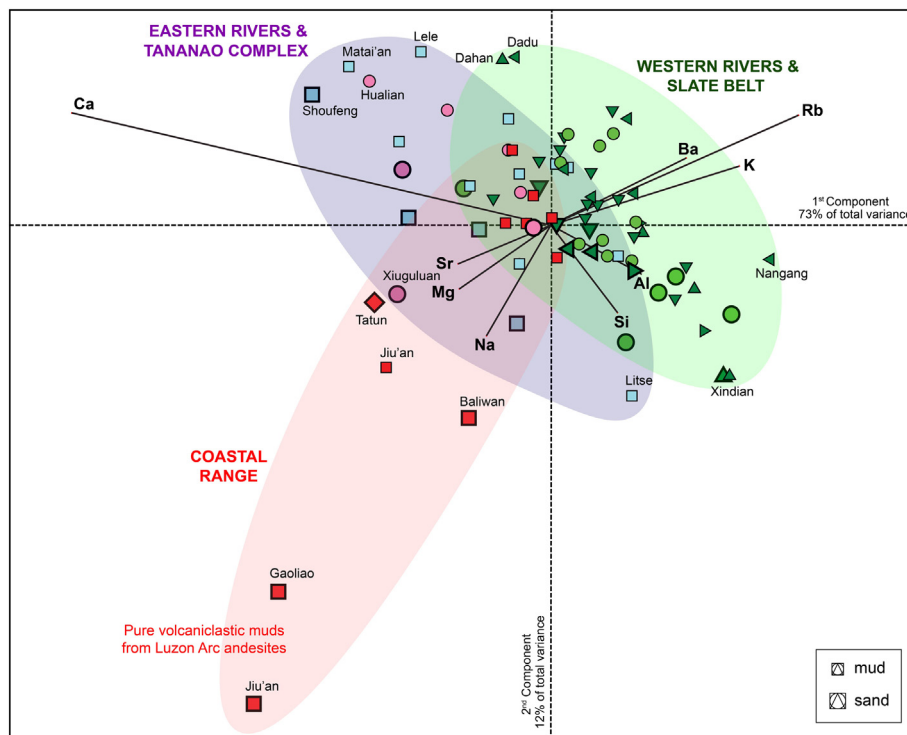


Fig. 5. Provenance discrimination based on elemental geochemistry (muds, smaller symbols; sands, larger symbols; provenance groups as in Table 1). Sediments of eastern Taiwan derived from the Tananao Complex and/or Coastal Range andesites are richer in Ca, Sr, Mg, and Na. In the rest of Taiwan, sediments largely derived from the Slate Belt and/or Western Foothills are instead richer in K, Rb, and Ba (compare with fig. 10 in Garzanti and Resentini, 2016). The compositional biplot (Gabriel, 1971) discriminates among sample groups and at the same time highlights the relationships among variables in bidimensional space.

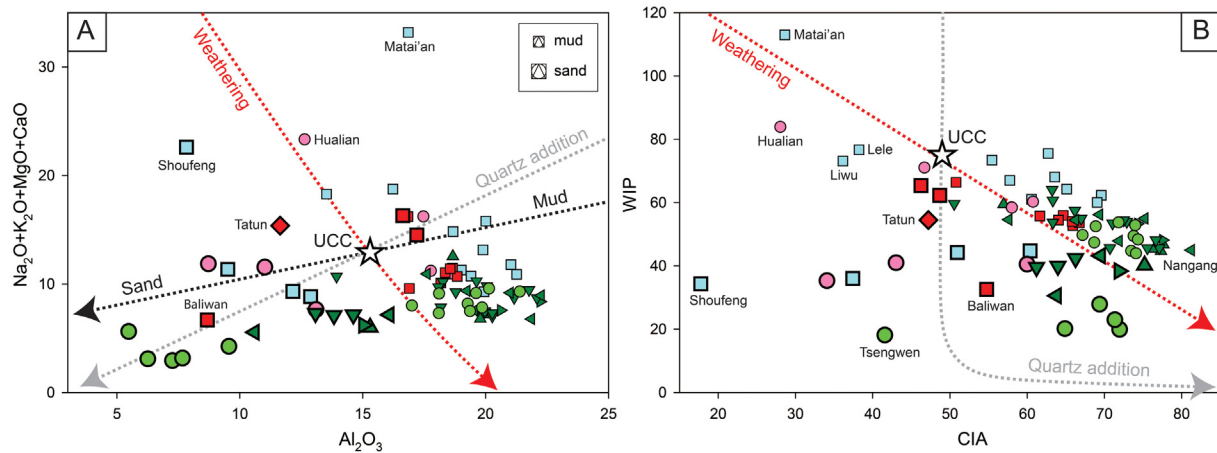


Fig. 6. Discriminating the effects of (inherited) weathering, recycling, and grain size (muds, smaller symbols; sands, larger symbols; provenance groups as in Table 1). The quartz-addition trend is calculated by progressively adding (or subtracting) SiO_2 to the UCC standard composition, the weathering trend by progressively subtracting mobile metals while assuming Si and Al unchanged, and the grain-size trend is based on data from Alpine and Himalayan sediments (Garzanti et al., 2010, 2011, 2012). A) The Al vs. mobile-elements plot mainly reflects the grain-size effect, separating sands more strongly affected by quartz addition from muds more strongly affected by (inherited) weathering. B) The CIA/WIP plot mainly reflects the influence of source-rock lithology and scarcity of quartz-rich rocks in Taiwan: i) quartz addition is most evident for western river sands draining the Western Foothills and for Baliwan sand recycling Pliocene-Pleistocene sandstones of the Coastal Range; ii) low CIA and high WIP characterizes rivers draining the Tailuko marbles and metabasites in eastern Taiwan and Pleistocene limestones in western Taiwan; iii) high CIA identifies sediments generated in the axial Slate Belt, where exposed mudrocks reflect Cenozoic paleoweathering on mainland China.

from mudrocks originally generated in wet mainland China and accumulated along the Chinese passive margin before being tectonically accreted to the Western Foothills of the Taiwan thrust belt (Lin et al., 2003). These sedimentary rocks were originally fed by the Yangtze River (Garzanti et al., 2021b), which today carries significant amounts of kaolinite to the sea (21 ± 3 % of the clay-mineral assemblage; He et al., 2013). Evidence for more intense chemical weathering in western Taiwan than in eastern Taiwan is thus dubious. Instead, the relatively high kaolinite content in Jingmei River mud, coupled with the relatively high illite chemistry index (0.42), may hint at present kaolinite formation in the wetter conditions of northern Taiwan (Li et al., 2012) (Fig. 2).

5.2. Insights from geochemistry

The mobility of alkali and alkaline-earth metals has been traditionally employed to assess the severity of chemical weathering, although detangling the effect of weathering from that of source-rock lithology is far from straightforward (Dinis et al., 2017). In sediments generated today on Taiwan Island, the concentration of chemical elements is principally controlled by provenance rather than by climate-induced weathering (Garzanti and Resentini, 2016) (Fig. 5). Mg and Ca are even strongly enriched relative to the UCC in muds of eastern Taiwan rivers draining marbles and metabasites of the Tailuko Belt ($\alpha^{\text{Al}}\text{Mg}$ as low as 0.3–0.6, $\alpha^{\text{Al}}\text{Ca}$ as low as 0.2–0.3, and CIA as low as 28–36 in Liwu, Hualian, and Matalai'an muds) (Table 2). Conversely, the highest CIA values are observed in mud derived from the Hsuehshan Range, largely consisting of Eocene-Oligocene mudrocks (Fig. 6). Such a signature is inferred to reflect weathering inherited from recycling of mainly Paleocene sedimentary rocks of the Hsuehshan Range, originally generated on the Chinese mainland at a time of globally warmer and more humid greenhouse climatic conditions, and fed from coastal rivers draining the Cathaysia Block (Deng et al., 2017; Garzanti et al., 2021b). At present, CIA indices are as high as 90 in river muds of coastal South China on the western side of the Taiwan Strait, characterized by warm-wet monsoonal climate (He et al., 2020).

5.3. The modern-sediment lesson

Clay mineralogy and elemental geochemistry are widely used, unfortunately too often uncritically, to infer conditions of weathering at the time of sedimentation (e.g., Nesbitt and Young, 1982; Price and Velbel, 2003). Studies of modern sediments worldwide, however, have

conclusively documented that source-rock lithology plays a decisive role and that weathering features can be largely inherited from past sedimentary cycles (e.g., Borges et al., 2008; Li and Yang, 2010). The use of so-called weathering indices such as the CIA may thus be misleading, because the concentration of mobile alkali or alkaline-earth elements in the sediment is largely controlled by the composition of source rocks. Far superior is the use of $\alpha^{\text{Al}}\text{E}$ indices, which allow full detection of provenance-related effects. In a regime of extensive weathering, all mobile elements are expected to be depleted in a predictable order of mobility (typically Na and Ca more depleted than Mg and Sr, with K, Rb, and Ba less strongly depleted; Garzanti et al., 2013b; Dinis et al., 2020). This is not the case in Taiwan, where mobile elements preferentially hosted in phyllosilicates (K, Rb, Ba) are undepleted to mildly depleted in rivers draining mudrocks exposed in the Slate Belt and Western Foothills, whereas mobile elements contained in andesite, metabasite, and carbonate rocks (Mg, Ca) are even strongly enriched in rivers draining the Coastal Range and Tananao Complex.

Understanding whether a clay-mineral assemblage reflects present or past conditions of weathering is more difficult than detecting the effect of source-rock lithology. Emblematic is the case of the Kalahari Desert of southern Africa, where modern sediments contain significant amounts of kaolinite recycled from older deposits generated in wetter conditions at lower subequatorial latitudes and presently carried by rivers southward into the dryland (Garzanti et al., 2022a). A similar phenomenon is observed all across tropical southern Africa from Namibia to Mozambique, where kaolinite is mainly recycled from relic lateritic paleosols and duricrusts formed during Cretaceous to Cenozoic peneplanation phases rather than from recent soil profiles (Garzanti et al., 2014, 2022b).

The study of modern sedimentary systems tells us that geochemical or mineralogical indices cannot be simplistically used to interpret climatic and weathering regimes without a careful inspection of independent proxies and an accurate knowledge of regional geological history and areal distribution of source-rock types. Far from straightforwardly obtained even for recent sediments, correct inferences require full consciousness in the case of speculative paleoclimatic and paleogeographic reconstructions.

6. Clay from land to ocean

A comparison of clay-mineral assemblages in Taiwan rivers and offshore deep-sea deposits gives us a key to trace transport pathways and

the relative influence of gravity flows and oceanic currents. The distribution of clay-mineral assemblages in different deep-sea provinces all around Taiwan was documented in previous studies (J.P. Liu et al., 2008a; Z. Liu et al., 2008b; Wan et al., 2010a, 2010b) and thoroughly illustrated in Nayak et al. (2021).

Besides Taiwan Island and mainland China, two major sources were identified in the Ryukyu arc to the north and in the Luzon arc to the south, both chiefly supplying smectite from alteration of volcanic rocks (Fig. 7). Sediments in the Ryukyu subduction zone contain more chlorite than other deep-sea provinces, revealing major input from northeastern Taiwan rivers draining the Tananao Complex (e.g., Dong'aobei, Heping, and Nanao) via the river-connected Heping Canyon (Fig. 7). Deep-sea sediments offshore eastern Taiwan are smectite-rich, reflecting major supply from volcanic rocks of the Coastal Range. Deep-sea sediments offshore southwestern Taiwan are mostly rich in illite and smectite. A major exception is the Gaoping Canyon, where large volumes of mud rich in illite and chlorite shed from the Backbone Range widely exposed in the catchment of the Gaoping River and transported by all its major tributaries (e.g., Ailiao, Koushe, Zhuokou, Laonong, and Qishan) are conveyed to the northern South China Sea.

In mainland China, the most important sediment source by far is the Yangtze River, which carries 56–65 % illite, 17–23 % kaolinite, 17–20 % chlorite, and <4 % smectite to the southwestern East China Sea (He et al., 2013). About one third of Yangtze suspended sediment is estimated to be trapped in the inner shelf and transported southward

along the coast, mostly by the China (Zhemu) Coastal Current during winter months. These sediments have formed a coastal mud wedge extending southward for ~800 km as far as the latitude of central Taiwan but no more than ~100 km across the Chinese continental shelf (Liu et al., 2006).

Rivers draining the Fujian and Zhejiang Provinces of southeast China between the Yangtze and Pearl River mouths reach peak discharge during tropical storms in summer and carry mostly illite and chlorite in the north (Bi et al., 2015) and mostly kaolinite in the south (Liu et al., 2016) (Fig. 7). Because their combined sediment load is one-order-of-magnitude less than the Yangtze River load and is mostly sequestered within or near the estuaries, supply to the Taiwan Strait by these rivers is considered to be negligible (J.P. Liu et al., 2008a). The Pearl River, the major river draining into the northern South China Sea, carries abundant kaolinite, associated with illite, chlorite, and minor smectite (Liu et al., 2007a, 2007b; He et al., 2020). Sediment supply from mainland China thus appears to be largely limited to the proximal continental margins of the East China Sea, Taiwan Strait, and South China Sea, and thus of lesser importance relative to Taiwan rivers for deep-sea muds accumulating offshore Taiwan (J.P. Liu et al., 2008a; Wan et al., 2010b).

7. Conclusions

The present study illustrates the areal distribution of clay minerals (illite, chlorite, smectite, and kaolinite), clay mineral indices (illite

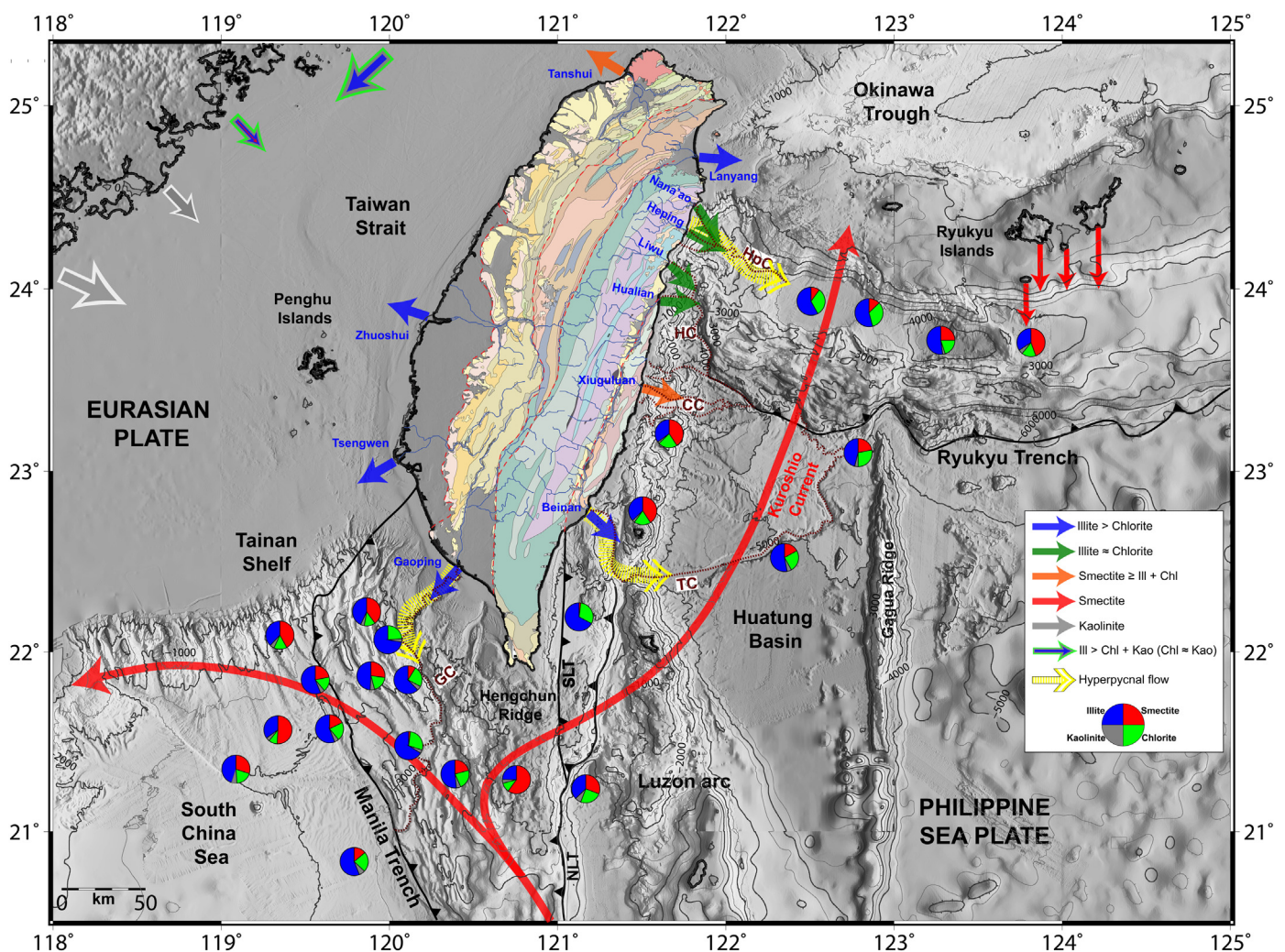


Fig. 7. A synopsis of mud transport from Taiwan rivers to the Philippine and South China seas (clay-mineral data on deep-sea muds after Nayak et al., 2021). Canyons: CC, Chimei; GC, Gaoping; HC, Hualien; HpC, Heping; TC, Taitung. NLT, North Luzon Trough; SLT, Southern Longitudinal Trough.

crystallinity and illite chemistry), major and trace elements, and chemical indices ($\alpha^{Al}E$ and CIA values) in river muds generated within and dispersed around Taiwan Island. Mineralogical and geochemical signatures allow a clear distinction among source areas, testifying to dominant provenance control and mostly inherited weathering features. Among clay minerals, illite is primarily generated from Paleogene slates exposed in the Backbone and Hsuehshan ranges and from Neogene shales exposed in the Western Foothills, chlorite mainly from schists and metabasites of the Tananao Complex, and smectite from arc andesites of the Coastal Range. Kaolinite, negligible in eastern Taiwan, is minor but significant in western Taiwan, where it is largely recycled from mudrocks of the Western Foothills.

Among chemical elements, Mg and Ca are enriched relative to the UCC standard in river sediments of eastern Taiwan, and especially in muds derived from marbles and metabasites of the Tananao Complex and volcanic rocks of the Coastal Range, but moderately to strongly depleted in river muds from western and northern Taiwan recycled from Cenozoic mudrocks originally generated in hot and humid eastern South China. Evidence for a difference in chemical weathering between eastern Taiwan and western Taiwan, where the climate is somewhat drier but rivers are longer and less steep, is questionable. Only locally (i.e., Jingmei River mud) do the relatively high kaolinite content and Illite Chemistry index hint at present kaolinite formation in well-drained soils developed in the wetter conditions of northern Taiwan.

Clay mineralogy provides a robust provenance tracer of mud generated in Taiwan and transported offshore to the abyssal floors of the Philippine and South China seas. Mostly illite is supplied to the Taiwan Strait and the South China Sea, whereas subequal amounts of illite and chlorite are delivered from northeastern Taiwan rivers draining the Tananao Complex to the Ryukyu forearc basin (Fig. 7). Smectite from Coastal Range andesites is transferred via the Xiugulan River and Chimei Canyon directly to the Ryukyu trench. Additional amounts of smectite produced in the Ryukyu and Luzon arcs are transported southward to the Ryukyu forearc basin and northward by the Kuroshio Current, northwestward to the northern South China Sea, and north-eastward to the Huatung Basin and Okinawa Trough.

Declaration of competing interest

The authors declare that they have no known competing financial interests or personal relationships that could have appeared to influence the work reported in this paper.

Acknowledgments

We heartily thank Pei-Hua Hsu and Ming-Wei Liao for fundamental assistance in the field. Sampling was funded by Swiss National Science Foundation grant #200020-131890 to Sebastien Castellort. Editor Catherine Chagué and two anonymous reviewers provided careful constructive comments.

Appendix A. Supplementary data

Supplementary materials associated with this article, including information on all studied Taiwan sediment samples (Table A1), grain size (Table A2), clay mineralogy (Table A3), mud geochemistry (Table A4), and sand geochemistry (Table A5) are found online at <https://doi.org/10.1016/j.sedgeo.2022.106199>. The Google-Earth map of sampling sites Taiwan Clay.kmz is also provided.

References

Bi, L., Yang, S.Y., Li, C., Guo, Y.L., Wang, Q., Liu, J.T., Yin, P., 2015. Geochemistry of river-borne clays entering the East China Sea indicates two contrasting types of weathering and sediment transport processes. *Geochemistry, Geophysics, Geosystems* 16, 3034–3052.

- Biscaye, P.E., 1965. Mineralogy and sedimentation of recent deep-sea clay in the Atlantic Ocean and adjacent seas and oceans. *Geological Society of America Bulletin* 76, 803–832.
- Borges, J.B., Huh, Y., Moon, S., Noh, H., 2008. Provenance and weathering control on river bed sediments of the eastern Tibetan Plateau and the Russian Far East. *Chemical Geology* 254, 52–72.
- Boulay, S., Colin, C., Trentesaux, A., Pluquet, F., Bertaux, J., Blamart, D., Buehring, C., Wang, P., 2003. Mineralogy and sedimentology of Pleistocene sediment in the South China Sea (ODP Site 1144). In: Prell, W., Wang, P., Blum, P., Rea, D., Clemens, S. (Eds.), *Proceedings of the Ocean Drilling Program. Scientific Results* 184, pp. 1–21.
- Byrne, T., Chan, Y.C., Rau, R.J., Lu, C.Y., Lee, Y.H., Wang, Y.J., 2011. The arc–continent collision in Taiwan. *Arc–Continent Collision*. Springer, Berlin, pp. 213–245.
- Chamley, H., 1989. *Clay Sedimentology*. Springer, New York (623 pp.).
- Chamley, H., Angelier, J., Teng, L.S., 1993. Tectonic and environmental control of the clay mineral sedimentation in the late Cenozoic orogen of Taiwan. *Geodinamica Acta* 6, 135–147.
- Chang, C.P., Angelier, J., Huang, C.Y., 2000. Origin and evolution of a melange: the active plate boundary and suture zone of the Longitudinal Valley, Taiwan. *Tectonophysics* 325, 43–62.
- Chen, C.H., 2000. Geologic Map of Taiwan, Scale 1:500,000.
- Clark, M.K., Schoenbohm, L.M., Royden, L.H., Whipple, K.X., Burchfiel, B.C., Zhang, X., Tang, W., Wang, E., Chen, L., 2004. Surface uplift, tectonics, and erosion of eastern Tibet from large-scale drainage patterns. *Tectonics* 23, TC1006. <https://doi.org/10.1029/2002TC001402>.
- Clift, P.D., Carter, A., Campbell, I.H., Pringle, M.S., Van Lap, N., Allen, C.M., Hodges, K.V., Tan, M.T., 2006a. Thermochronology of mineral grains in the Red and Mekong Rivers, Vietnam: provenance and exhumation implications for Southeast Asia. *Geochemistry, Geophysics, Geosystems* 7, Q10005. <https://doi.org/10.1029/2006GC001336>.
- Clift, P.D., Blusztajn, J., Nguyen, A.D., 2006b. Large-scale drainage capture and surface uplift in eastern Tibet–SW China before 24 Ma inferred from sediments of the Hanoi Basin, Vietnam. *Geophysical Research Letters* 33, L19403. <https://doi.org/10.1029/2006GL027772>.
- Dadson, S.J., Hovius, N., Chen, H., Dade, W.B., Hsieh, M.L., Willett, S.D., Hu, J.C., Horng, M.J., Chen, M.C., Stark, C.P., Lague, D., Lin, J.C., 2003. Links between erosion, runoff variability and seismicity in the Taiwan orogen. *Nature* 426, 648–651.
- Dadson, S.J., Hovius, N., Pegg, S., Dade, W.B., Horng, M.J., Chen, H., 2005. Hyperpycnal river flows from an active mountain belt. *Journal of Geophysical Research: Earth Surface* 110, F04016. <https://doi.org/10.1029/2004JF000244>.
- Das, P., Lin, A.T.S., Chen, M.P.P., Miramontes, E., Liu, C.S., Huang, N.W., Kung, J., Hsu, S.K., Pillutla, R.K., Nayak, K., 2021. Deep-sea submarine erosion by the Kuroshio current in the Manila accretionary prism, offshore Southern Taiwan. *Tectonophysics* 807, 228813. <https://doi.org/10.1016/j.tecto.2021.228813>.
- Defant, M.J., Maury, R., Joron, J.L., Feigenson, M.D., Leterrier, J., Bellon, H., Jacques, D., Richard, M., 1990. The geochemistry and tectonic setting of the northern section of the Luzon arc (the Philippines and Taiwan). *Tectonophysics* 183, 187–205.
- Deng, K., Yang, S., Li, C., Su, N., Bi, L., Chang, Y.P., Chang, S.C., 2017. Detrital zircon geochronology of river sands from Taiwan: implications for sedimentary provenance of Taiwan and its source link with the east China mainland. *Earth-Science Reviews* 164, 31–47.
- Deng, K., Yang, S., von Blanckenburg, F., Wittmann, H., 2020. Denudation rate changes along a fast-eroding mountainous river with slate headwaters in Taiwan from ^{10}Be (meteoric)/ 9Be ratios. *Journal of Geophysical Research: Earth Surface* 125, e2019JF005251. <https://doi.org/10.1029/2019JF005251>.
- Deng, K., Wittmann, H., Yang, S., von Blanckenburg, F., 2021. The upper limit of denudation rate measurement from cosmogenic ^{10}Be (meteoric)/ 9Be ratios in Taiwan. *Journal of Geophysical Research: Earth Surface* 126, e2021JF006221. <https://doi.org/10.1029/2021JF006221>.
- Dinis, P., Garzanti, E., Vermeesch, P., Huvi, J., 2017. Climatic zonation and weathering control on sediment composition (Angola). *Chemical Geology* 467, 110–121.
- Dinis, P.A., Garzanti, E., Hahn, A., Vermeesch, P., Cabral-Pinto, M., 2020. Weathering indices as climate proxies. A step forward based on Congo and SW African river muds. *Earth-Science Reviews* 201, 103039. <https://doi.org/10.1016/j.earscirev.2019.103039>.
- Dorsey, R.J., 1988. Provenance evolution and unroofing history of a modern arc–continent collision: evidence from petrography of Plio–Pleistocene sandstones, eastern Taiwan. *Journal of Sedimentary Petrology* 58, 208–218.
- Dorsey, R.J., Buchovecky, E.J., Lundberg, N., 1988. Clay mineralogy of Pliocene–Pleistocene mudstones, eastern Taiwan: combined effects of burial diagenesis and provenance unroofing. *Geology* 16, 944–947.
- Ernst, W.G., Jahn, B.M., 1987. Crustal accretion and metamorphism in Taiwan, a post-Palaeozoic mobile belt. *Philosophical Transactions of the Royal Society of London, Series A, Mathematical and Physical Sciences* 321, 129–161.
- Fuller, C.W., Willett, S.D., Fisher, D., Lu, C.Y., 2006. A thermomechanical wedge model of Taiwan constrained by fission-track thermochronometry. *Tectonophysics* 425, 1–24.
- Gabriel, K.R., 1971. The biplot graphic display of matrices with application to principal component analysis. *Biometrika* 58, 453–467.
- Gaillardet, J., Dupré, B., Louvat, P., Allègre, C.J., 1999. Global silicate weathering and CO_2 consumption rates deduced from the chemistry of large rivers. *Chemical Geology* 159, 3–30.
- Garzanti, E., Resentini, A., 2016. Provenance control on chemical indices of weathering (Taiwan river sands). *Sedimentary Geology* 336, 81–95.
- Garzanti, E., Andò, S., France-Lanord, C., Vezzoli, G., Najman, Y., 2010. Mineralogical and chemical variability of fluvial sediments. 1. Bedload sand (Ganga–Brahmaputra, Bangladesh). *Earth and Planetary Science Letters* 299, 368–381.
- Garzanti, E., Andò, S., France-Lanord, C., Galy, V., Censi, P., Vignola, P., 2011. Mineralogical and chemical variability of fluvial sediments. 2. Suspended-load silt (Ganga–Brahmaputra, Bangladesh). *Earth and Planetary Science Letters* 302, 107–120.

- Garzanti, E., Resentini, A., Vezzoli, G., Ando, S., Malusa, M., Padoan, M., 2012. Forward compositional modelling of Alpine orogenic sediments. *Sedimentary Geology* 280, 149–164.
- Garzanti, E., Padoan, M., Andò, S., Resentini, A., Vezzoli, G., Lustrino, M., 2013a. Weathering and relative durability of detrital minerals in equatorial climate: sand petrology and geochemistry in the East African Rift. *The Journal of Geology* 121, 547–580.
- Garzanti, E., Padoan, M., Setti, M., Najman, Y., Peruta, L., Villa, I.M., 2013b. Weathering geochemistry and Sr-Nd fingerprints of equatorial upper Nile and Congo muds. *Geochemistry, Geophysics, Geosystems* 14, 292–316.
- Garzanti, E., Padoan, M., Setti, M., López-Galindo, A., Villa, I.M., 2014. Provenance versus weathering control on the composition of tropical river mud (southern Africa). *Chemical Geology* 366, 61–74.
- Garzanti, E., Vermeesch, P., Vezzoli, G., Andò, S., Botti, E., Limonta, M., Dinis, P., Hahn, A., Baudet, D., De Grave, J., Yaya, N.K., 2019. Congo River sand and the equatorial quartz factory. *Earth-Science Reviews* 197, 102918. <https://doi.org/10.1016/j.earscirev.2019.102918>.
- Garzanti, E., He, J., Barbarano, M., Resentini, A., Li, C., Yang, L., Wang, S., Wang, H., 2021a. Provenance versus weathering control on sediment composition in tropical monsoonal climate (South China) 2. Sand petrology and heavy minerals. *Chemical Geology* 564, 119997. <https://doi.org/10.1016/j.chemgeo.2020.119997>.
- Garzanti, E., Barbarano, M., Andò, S., Lenzi, M., Deng, K., Yang, S., 2021b. Provenance of Neogene sandstones in western Taiwan traced with garnet geochemistry and zircon geochronology. *Basin Research* 33, 2069–2088.
- Garzanti, E., Pastore, G., Stone, A., Vainer, S., Vermeesch, P., Resentini, A., 2022a. Provenance of Kalahari Sand: paleoweathering and recycling in a linked fluvial-aeolian system. *Earth-Science Reviews* 224, 103867.
- Garzanti, E., Bayon, G., Dinis, P., Vermeesch, P., Pastore, G., Resentini, A., Barbarano, M., Ncube, L., Van Niekerk, H.J., 2022b. The segmented Zambezi sedimentary system from source to Sink: 2. geochemistry, clay minerals, and detrital geochronology. *The Journal of Geology* 130 (3), 171–208 available online at <https://www.journals.uchicago.edu/doi/10.1086/719166>.
- He, M., Zheng, H., Huang, X., Jia, J., Li, L., 2013. Yangtze River sediments from source to sink traced with clay mineralogy. *Journal of Asian Earth Sciences* 69, 60–69.
- He, J., Garzanti, E., Dinis, P., Yang, S., Wang, H., 2020. Provenance versus weathering control on sediment composition in tropical monsoonal climate (South China) 1. Geochemistry and clay mineralogy. *Chemical Geology* 558, 119860. <https://doi.org/10.1016/j.chemgeo.2020.119860>.
- Hovius, N., Meunier, P., Lin, C.W., Chen, H., Chen, Y.G., Dadson, S., Horng, M.J., Lines, M., 2011. Prolonged seismically induced erosion and the mass balance of a large earthquake. *Earth and Planetary Science Letters* 304, 347–355.
- Huang, P.H., Wei, C., Zhang, J., 2021. High-P metamorphism of garnet-epidote-amphibole schists from the Yuli Belt, Eastern Taiwan: evidence related to warm subduction. *Journal of Metamorphic Geology* 39, 675–693.
- Keyser, W., Tsai, C.H., Iizuka, Y., Oberhänsli, R., Ernst, W.G., 2016. High-pressure metamorphism in the Chinshuichi area, Yuli belt, eastern Taiwan. *Tectonophysics* 692, 191–202.
- Kottek, M., Grieser, J., Beck, C., Rudolf, B., Rubel, F., 2006. Worldmap of the Köppen-Geiger climate classification updated. *Meteorologische Zeitschrift* 15, 259–263.
- Lai, Y.M., Song, S.R., Lo, C.H., Lin, T.H., Chu, M.F., Chung, S.L., 2017. Age, geochemical and isotopic variations in volcanic rocks from the Coastal Range of Taiwan: implications for magma generation in the Northern Luzon Arc. *Lithos* 272, 92–115.
- Li, C., Yang, S., 2010. Is chemical index of alteration (CIA) a reliable proxy for chemical weathering in global drainage basins? *American Journal of Science* 310, 111–127.
- Li, C., Shi, X., Kao, S., Chen, M., Liu, Y., Fang, X., Lü, H., Zou, J., Liu, S., Qiao, S., 2012. Clay mineral composition and their sources for the fluvial sediments of Taiwanese rivers. *Chinese Science Bulletin* 57, 673–681.
- Lin, A.T., Watts, A.B., 2002. Origin of the West Taiwan Basin by orogenic loading and flexure of a rifted continental margin. *Journal of Geophysical Research: Solid Earth* 107, ETG-2. <https://doi.org/10.1029/2001JB000669>.
- Lin, A.T., Watts, A.B., Hesselbo, S.P., 2003. Cenozoic stratigraphy and subsidence history of the South China Sea margin in the Taiwan region. *Basin Research* 15, 453–478.
- Lin, A.T., Yang, C.-C., Wang, M.-H., Wu, J.-C., 2021. Oligocene-Miocene sequence stratigraphy in the northern margin of the South China Sea: an example from Taiwan. *Journal of Asian Earth Sciences* 213, 104765. <https://doi.org/10.1016/j.jseas.2021.104765>.
- Liu, Z., Trentesaux, A., Clemens, S.C., Wang, P., 2003. Quaternary clay mineralogy in the northern South China Sea (ODP Site 1146): implications for oceanic current transport and East Asian monsoon evolution. *Science in China Series D: Earth Science* 46, 1223–1235.
- Liu, Z., Colin, C., Trentesaux, A., Siani, G., Frank, N., Blamart, D., Farid, S., 2005. Late Quaternary climatic control on erosion and weathering in the eastern Tibetan Plateau and the Mekong Basin. *Quaternary Research* 63, 316–328.
- Liu, J.P., Li, A.C., Xu, K.H., Vellozzi, D.M., Yang, Z.S., Milliman, J.D., DeMaster, D.J., 2006. Sedimentary features of the Yangtze River-derived along-shelf clinoform deposit in the East China Sea. *Continental Shelf Research* 26, 2141–2156.
- Liu, Z., Colin, C., Huang, W., Chen, Z., Trentesaux, A., Chen, J., 2007a. Clay minerals in surface sediments of the Pearl River drainage basin and their contribution to the South China Sea. *Chinese Science Bulletin* 52, 1101–1111.
- Liu, Z., Colin, C., Huang, W., Le, K.P., Tong, S., Chen, Z., Trentesaux, A., 2007b. Climatic and tectonic controls on weathering in South China and the Indochina Peninsula: clay mineralogical and geochemical investigations from the Pearl, Red, and Mekong drainage basins. *Geochemistry, Geophysics, Geosystems* 8, Q05005. <https://doi.org/10.1029/2006GC001490>.
- Liu, J.P., Liu, C.S., Xu, K.H., Milliman, J.D., Chiu, J.K., Kao, S.J., Lin, S.W., 2008a. Flux and fate of small mountainous rivers derived sediments into the Taiwan Strait. *Marine Geology* 256, 65–76.
- Liu, Z., Tuo, S., Colin, C., Liu, J.T., Huang, C.Y., Selvaraj, K., Chen, C.T.A., Zhao, Y., Siringan, F.P., Boulay, S., Chen, Z., 2008b. Detrital fine-grained sediment contribution from Taiwan to the northern South China Sea and its relation to regional ocean circulation. *Marine Geology* 255, 149–155.
- Liu, Z., Colin, C., Li, X., Zhao, Y., Tuo, S., Chen, Z., Liu, J., Huang, C.-Y., You, C.-F., Huang, K.-F., 2010. Clay mineral distribution in surface sediments of the northeastern South China Sea and surrounding fluvial drainage basins: source and transport. *Marine Geology* 277, 48–60.
- Liu, Z.F., Zhao, Y.L., Colin, C., Statterger, K., Wiesner, M.G., Huh, C.A., Zhang, Y.W., Li, X.J., Sompongchaiyakul, P., You, C.F., Huang, C.Y., Liu, J.T., Siringan, F.P., Le, K.P., Sathiamurthy, E., Hantoro, W.S., Liu, J.G., Tuo, S.T., Zhao, S.H., Zhou, S.W., He, Z.D., Wang, Y.C., Bunsomboonsakul, S., Li, Y.L., 2016. Source-to-sink transport processes of fluvial sediments in the South China Sea. *Earth-Science Reviews* 153, 238–273.
- Milliman, J.D., Syvitski, J.P., 1992. Geomorphic/tectonic control of sediment discharge to the ocean: the importance of small mountainous rivers. *The Journal of Geology* 100, 525–544.
- Montgomery, D.R., Huang, M.Y.F., Huang, A.Y.L., 2014. Regional soil erosion in response to land use and increased typhoon frequency and intensity, Taiwan. *Quaternary Research* 81, 15–20.
- Nagel, S., Castellort, S., Garzanti, E., Lin, A.T., Willett, S.D., Mouthereau, F., Limonta, M., Adatte, T., 2014. Provenance evolution during arc-continent collision: sedimentary petrography of Miocene to Pleistocene sediments in the western foreland basin of Taiwan. *Journal of Sedimentary Research* 84, 513–528.
- Nagel, S., Granjeon, D., Willett, S., Lin, A.T.S., Castellort, S., 2018. Stratigraphic modeling of the Western Taiwan foreland basin: sediment flux from a growing mountain range and tectonic implications. *Marine and Petroleum Geology* 96, 331–347.
- Nayak, K., Lin, A.T.S., Huang, K.F., Liu, Z., Babonneau, N., Ratzov, G., Pillutla, R.K., Das, P., Hsu, S.K., 2021. Clay-mineral distribution in recent deep-sea sediments around Taiwan: Implications for sediment dispersal processes. *Tectonophysics* 814, 228974. <https://doi.org/10.1016/j.tecto.2021.228974>.
- Nesbitt, H.W., Young, G.M., 1982. Early Proterozoic climates and plate motions inferred from major element chemistry of lutites. *Nature* 299, 715–717.
- Nesbitt, H.W., Young, G.M., 1984. Prediction of some weathering trends of plutonic and volcanic rocks based on thermodynamic and kinetic considerations. *Geochimica et Cosmochimica Acta* 48, 1523–1534.
- Nesbitt, H.W., Young, G.M., 1989. Formation and diagenesis of weathering profiles. *The Journal of Geology* 97, 129–147.
- Pai, C.W., Wang, M.K., Chiu, C.Y., 2007. Clay mineralogical characterization of a toposequence of perhumid subalpine forest soils in northeastern Taiwan. *Geoderma* 138, 177–184.
- Parker, A., 1970. An index of weathering for silicate rocks. *Geological Magazine* 107, 501–504.
- Price, J.R., Velbel, M.A., 2003. Chemical weathering indices applied to weathering profiles developed on heterogeneous felsic metamorphic parent rocks. *Chemical Geology* 202, 397–416.
- Raymo, M.E., Ruddiman, W.F., Froelich, P.N., 1988. Influence of late Cenozoic mountain building on ocean geochemical cycles. *Geology* 16, 649–653.
- Resentini, A., Goren, L., Castellort, S., Garzanti, E., 2017. Partitioning sediment flux by provenance and tracing erosion patterns in Taiwan. *Journal of Geophysical Research: Earth Surface* 122, 1430–1454.
- Rudnick, R.L., Gao, S., 2003. Composition of the continental crust. In: Rudnick, R.L., Holland, H.D., Turekian, K.K. (Eds.), *Treatise on Geochemistry*. The Crust. 3. Elsevier Pergamon, Oxford, pp. 1–64.
- Schoenbohm, L.M., Whipple, K.X., Burchfiel, B.C., Chen, L., 2004. Geomorphic constraints on surface uplift, exhumation, and plateau growth in the Red River region, Yunnan Province, China. *Geological Society of America Bulletin* 116, 895–909.
- Selvaraj, K., Chen, C.T.A., 2006. Moderate chemical weathering of sub-tropical Taiwan: constraints from solid-phase geochemistry of sediments and sedimentary rocks. *The Journal of Geology* 114, 101–116.
- Shao, J., Yang, S., Li, C., 2012. Chemical indices (CIA and WIP) as proxies for integrated chemical weathering in China: inferences from analysis of fluvial sediments. *Sedimentary Geology* 265, 110–120.
- Shellnutt, J.G., Belousov, A., Belousova, M., Wang, K.L., Zellmer, G.F., 2014. Generation of calc-alkaline andesite of the Tatun volcanic group (Taiwan) within an extensional environment by crystal fractionation. *International Geology Review* 56, 1156–1171.
- Simoes, M., Beyssac, O., Chen, Y.G., 2012. Late Cenozoic metamorphism and mountain building in Taiwan: a review. *Journal of Asian Earth Sciences* 46, 92–119.
- Summerfield, M.A., Hulton, N.J., 1994. Natural controls of fluvial denudation rates in major world drainage basins. *Journal of Geophysical Research: Solid Earth* 99, 13871–13883.
- Suppe, J., 1981. The mechanics of mountain building and metamorphism in Taiwan. *Memoir of the Geological Society of China* 4, 67–89.
- Taylor, S.R., McLennan, S.M., 1995. The geochemical evolution of the continental crust. *Reviews of Geophysics* 33, 241–265.
- Teng, L., 1996. Extensional collapse of the northern Taiwan mountain belt. *Geology* 24, 949–952.
- Teng, L.S., Lin, A.T., 2004. Cenozoic tectonics of the China continental margin: insights from Taiwan. In: Malpas, J., Fletcher, C.J.N., All, J.R., Aitchison, J.C. (Eds.), *Aspects of the Tectonic Evolution of China*. Geological Society London, Special Publications 226, pp. 313–332.
- Wan, S., Cliff, P.D., Li, A., Li, T., Yin, X., 2010a. Geochemical records in the South China Sea: implications for East Asian summer monsoon evolution over the last 20 Ma. *Geological Society, London, Special Publication* 342 pp. 245–263.

- Wan, S., Li, A., Clift, P.D., Wu, S., Xu, K., Li, T., 2010b. Increased contribution of terrigenous supply from Taiwan to the northern South China Sea since 3 Ma. *Marine Geology* 278, 115–121.
- Wang, K.L., Chung, S.L., O'Reilly, S.Y., Sun, S.S., Shinjo, R., Chen, C.H., 2004. Geochemical constraints for the genesis of post-collisional magmatism and the geodynamic evolution of the northern Taiwan region. *Journal of Petrology* 45, 975–1011.
- Wilson, M.J., 1999. The origin and formation of clay minerals in soils: past, present and future perspectives. *Clay Minerals* 34, 7–25.
- Yu, N.T., Teng, L.S., Chen, W.S., Yue, L.F., Chen, M.M., 2013. Early post-rift sequence stratigraphy of a Mid-Tertiary rift basin in Taiwan: insights into a siliciclastic fill-up wedge. *Sedimentary Geology* 286, 39–57.
- Yui, T.F., Maki, K., Lan, C.Y., Hirata, T., Chu, H.T., Kon, Y., Yokoyama, T.D., Jahn, B.M., Ernst, W.G., 2012. Detrital zircons from the Tananao metamorphic complex of Taiwan: implications for sediment provenance and Mesozoic tectonics. *Tectonophysics* 541, 31–42.